Journal of Alloys and Compounds 509 (2011) 6227–6235

Contents lists available at ScienceDirect

Journal of Alloys and Compounds

journal homepage: www.elsevier.com/locate/jallcom

Effect of Nd_2O_3 addition on the surface phase of TiO_2 and photocatalytic activity studied by UV Raman spectroscopy

Mengqiong Yuan [a], Jing Zhang [a,*], Song Yan [a], Genxiang Luo [a], Qian Xu [b], Xiang Wang [b], Can Li [b]

[a] School of Chemistry and Materials Science, Liaoning Shihua University, Fushun 113001, Liaoning, China
[b] State Key Laboratory of Catalysis, Dalian Institute of Chemical Physics, Chinese Academy of Sciences, Dalian 116023, Liaoning, China

ARTICLE INFO

Article history:
Received 8 November 2010
Received in revised form 2 March 2011
Accepted 3 March 2011
Available online 10 March 2011

Keywords:
TiO_2 modified with Nd_2O_3
Co-precipitation method
Surface crystal phase
UV Raman spectroscopy
Photocatalysis

ABSTRACT

TiO_2 modified with Nd_2O_3 (Nd–TiO_2) nanoparticles were prepared by a co-precipitation method and utilized as the photocatalysts for the degradation of Rhodamine B (RhB). The influence of Nd_2O_3 on the bulk and surface phase, surface area, particle size, and optical response of TiO_2 was investigated by X-ray diffraction (XRD), UV Raman spectroscopy, transmission electron microscopy (TEM), BET, and UV–visible diffuse reflectance spectra. It is found that the crystalline phase and phase composition in the bulk and surface region of Nd–TiO_2 calcined at high temperatures can be tuned by changing the amount of Nd_2O_3. Based on the results from XPS, EDX, XRD, and UV Raman spectra, it is assumed that Nd^{3+} ions do not enter the TiO_2 lattice, but highly disperse onto the Nd–TiO_2 particle surface in the form of Nd_2O_3 crystallites. These crystallites inhibit the agglomeration, growth in crystal size, and anatase-to-rutile phase transformation of TiO_2. In the photocatalytic degradation of RhB reaction, Nd–TiO_2 nanoparticles with higher surface area and wider optical response are more reactive in case of the same surface anatase phase. When the mixed phases of anatase and rutile exist in the surface region of Nd–TiO_2, the synergetic effect over surface area and optical response is the important parameter which determines optimal photocatalytic activity.

1. Introduction

Titania (TiO_2) is widely used as an effective photocatalyst for the photodegradation of organic pollutants in water and air [1–3]. Anatase and rutile are TiO_2 polymorphic forms which are relevant in photocatalytic applications [4,5]. Anatase is usually considered to be more active than rutile. The photocatalytic activity and role of the rutile phase is still controversial. In general, the pure rutile phase has limited photocatalytic activity [6]. Some work [7–9] has demonstrated that rutile TiO_2 with a small crystal size and large surface area can possess high photocatalytic activity. Sclafani et al. [10] observed that the rutile phase is active or inactive according to preparation conditions.

Recent studies [11–15] suggest that the photocatalytic and photovoltaic properties of TiO_2 nanoparticles with mixed phases are better than pure anatase TiO_2. The high photocatalytic activity of the mixed phase TiO_2 such as P-25 (20% rutile, 80% anatase) could be attributed to the synergetic effect of the anatase and rutile particles. This effect was believed to involve photoexcited charge migration between the two phases that in turn enhances charge separation [16–18].

The surface properties [19] of TiO_2 intrinsically determine the surface separation and transfer of charge carriers by generating surface states, where electrons and holes are trapped and transferred for subsequent photocatalytic reaction. Our previous results [20–22] showed that UV Raman spectroscopy is more surface sensitive for TiO_2 than XRD because TiO_2 strongly absorbs UV light. It was found that phtocatalytic activity of TiO_2 for H_2 production from the photocatalytic reaction of water and methanol is dependent on its surface phase [22]. The phase junction formed between the surface anatase and rutile can greatly enhance photocatalytic H_2 evolution. We are interested in the following questions: can we control the surface phase of TiO_2 calcined at high temperature by a simple method? Is the surface phase of TiO_2 the main factor for its activity in photocatalytic degradation of organic pollutants?

Doping is used as a modification method for altering phase structure, electronic structure, and surface structure [23]. Doping with lanthanide allows one to tune the phase transformation, absorption properties, and photocatalytic activity of TiO_2 [24]. This paper attempts to control the surface phase of TiO_2 by neodymium oxide (Nd_2O_3) via a co-precipitation method. The influence of Nd_2O_3 on the surface and bulk crystalline phase, surface area, particle size, and optical response of TiO_2 was studied by UV Raman spectroscopy, XRD, TEM, XPS, SEM-EDX, and UV diffuse reflectance

* Corresponding author at: School of Chemistry and Materials Science, Liaoning Shihua University, P.O. Box 110, Fushun 113001, Liaoning, China.
Tel.: +86 413 6863390; fax: +86 413 6860548.
E-mail addresses: jingzhang.dicp@live.cn (J. Zhang), canli@dicp.ac.cn (C. Li).

0925-8388/$ – see front matter.
doi:10.1016/j.jallcom.2011.03.010

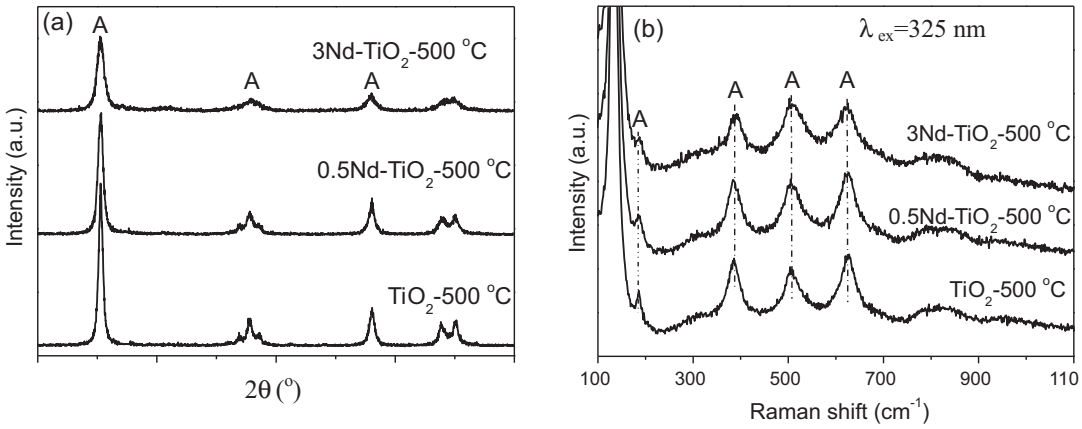

Fig. 1. The XRD patterns (a) and UV Raman spectra (b) of the TiO_2-500 °C and Nd–TiO_2-500 °C samples.

spectroscopy. Furthermore, we discuss how these results can be used to control the surface phase of TiO_2 calcined at high temperatures.

The influence of surface phase, surface area, particle size, and optical response of Nd–TiO_2 on the photocatalytic degradation of Rhodamine B (RhB) was investigated. It was found that the synergistic effect between surface anatase and rutile phase of Nd–TiO_2 plays an important role in determining optimal photocatalytic degradation of RhB, compared to the surface area and optical response parameters.

2. Experimental procedures

2.1. Materials

For all preparations, neodymiun nitrate ($Nd(NO_3)_3{\cdot}6H_2O$), titanium (IV) *n*-butoxide, anhydrous ethanol, and ammonia solution were of analytical grade and were used without further purification.

2.2. Characterization

UV Raman spectra were measured at room temperature with a Jobin-Yvon T64000 triple-stage spectrograph with spectral resolution of 2 cm^{-1}. A 325 nm He–Cd laser was used as an excitation source with an output power of 25 mW. X-ray powder diffraction (XRD) patterns were obtained on a Rigaku MiniFlex diffractometer with Cu Kα radiation source. Diffraction patterns were collected from 20° to 60° at a speed of 5° min^{-1}. Transmission electron microscopy (TEM) was taken on a JEOL 2000EX for estimating particle size and morphology. The morphologies were also examined by scanning electron microscopy (SEM) taken with a Quanta 200 FEG scanning electron microscope. Distribution of Ti and Nd concentration in the Nd–TiO_2 was analyzed by energy-dispersive X-ray spectroscopy (EDX, HAADF, FEI TECNAI G2 F30). Ultraviolet–visible diffuse reflectance spectra were recorded on a JASCO V-550 UV–Vis spectrophotometer. The Brunauer–Emmett–Teller (BET) surface areas of TiO_2 and Nd–TiO_2 samples were measured by nitrogen adsorption at 77 K using a Micromeritics ASAP 2000 adsorption analyzer.

The X-ray photoelectron spectroscopy (XPS) investigations were carried out on a spectrometer (VG ESCALAB MK-2) using Al Ka as the excitation source. The electron analyzer was operated at constant pass energy of 50 eV. The calibration of the binding-energy scale and the corrections of the energy shift as a result of the steady-state charging effect were accomplished by assuming that the C1s line, resulting from ubiquitous carbon produced from the pumping-oil vapor, lies at 284.6 eV.

2.3. Synthesis of TiO_2 modified with Nd_2O_3

TiO_2 modified with Nd_2O_3 (Nd–TiO_2), containing different amounts of Nd_2O_3 (0.5 wt% and 3 wt%), was prepared by a co-precipitation method. An amount of neodymiun nitrate was dissolved in 20 ml anhydrous ethanol. This solution was added slowly to a mixture solution of 50 ml titanium (IV) *n*-butoxide ($Ti(OBu)_4$) and 100 ml anhydrous ethanol. An ammonia solution was added to the above solution while stirring until the pH of the solution reached 9. The resulting white precipitate was stirred for 24 h, it was then washed twice with deionized water and anhydrous ethanol and subsequently dried at 100 °C for 12 h to obtain amorphous Nd–TiO_2.

To provide a comparison with the Nd–TiO_2 sample, amorphous TiO_2 was prepared via the same procedure without adding dopant. Amorphous Nd–TiO_2 and TiO_2 were calcined in air at 500 °C and 800 °C for 3 h, respectively. The TiO_2 samples with 0, 0.5, and 3 wt% Nd_2O_3 are denoted as TiO_2-500 °C (TiO_2-800 °C), 0.5Nd–TiO_2-500 °C (0.5Nd–TiO_2-800 °C), and 3Nd–TiO_2-500 °C (3Nd–TiO_2-800 °C), respectively.

2.4. Photocatalytic activity test

A set of photocatalytic degradation experiments were performed with the following procedure: photodegradation RhB was carried out in 100 ml Pyrex reactor filled with ion-exchanged water (60 ml) containing RhB (20 mg/l) and 0.05 g Nd–TiO_2 (or TiO_2) sample. The suspension was stirred for 30 min in the dark to obtain adsorption–desorption equilibrium of the dye before illumination. After irradiation with a 250 W high voltage mercury lamp (λ = 365 nm, Shanghai Yaming Lighting Co.), a 3 ml aliquot was taken after every 10 min and immediately centrifuged. The RhB concentration in the clear solution is analyzed by the optical characteristic absorption (22PC spectrophotometer, Shanghai Lengguang Technology Co., Ltd.) at the wavelength of 553 nm of RhB solution. The blank experiments without mercury lamp and without catalysts of RhB solution under the same condition are also compared in this study. The blank study shows that mere photolysis can be ignored for RhB. We also examined the activity of photodegradation of pure Nd_2O_3 (Pure Nd_2O_3 was obtained by calcining $Nd(NO_3)_3{\cdot}6H_2O$ at 500 °C for 3 h). It was found that Nd_2O_3 does not catalyze the degradation of RhB under our reaction conditions.

3. Results and discussion

3.1. The bulk and surface crystalline phase of Nd–TiO_2-500 °C

It is generally observed that TiO_2 nanoparticles tend to aggregate with each other to form bigger nanoparticles after calcination [25]. Thus, in the following discussion, the bulk and surface regions of TiO_2 and Nd–TiO_2 samples calcined at different temperatures actually refer to the inner bulk regions and outer surface regions of agglomerated particles, respectively. For all our samples, the crystalline phase in the bulk and surface region were characterized by XRD and UV Raman spectroscopy, respectively [20].

The diffraction peaks (25.5°, 37.9°, 48.2°, 53.8°, and 55.0°) [26] from the XRD results (Fig. 1a) indicate that bulk regions of TiO_2-500 °C and Nd–TiO_2-500 °C are in the anatase phase. For Nd–TiO_2-500 °C, the characteristic peaks of anatase TiO_2 decrease in intensity and increase in band width with increasing amounts of Nd_2O_3. The average crystallite sizes of TiO_2-500 °C, 0.5Nd–TiO_2-500 °C, and 3Nd–TiO_2-500 °C was calculated by using Scherrer's formula and determined to be about 20.2 nm, 16.3 nm, and 12.2 nm, respectively (Table 1). Compared with TiO_2, the doped TiO_2 particles have smaller size. Thus, the above changes in the XRD peaks can be attributed to a reduced grain size and a low extent of crystallinity of Nd–TiO_2-500 °C [27]. This suggests that doping Nd_2O_3 suppresses the growth of TiO_2 nanoparticles and crystallization of TiO_2.

Fig. 1b displays the UV Raman spectra of the TiO_2-500 °C and Nd–TiO_2-500 °C samples. The characteristic bands of anatase phase at 143, 195, 395, 515, and 638 cm^{-1} [28] are observed for all samples. These results indicate that the surface phases of TiO_2-500 °C and Nd–TiO_2-500 °C are in the anatase phase. Compared

Table 1
Crystallite size, rutile content in the bulk and surface region, and specific surface area of TiO_2 and Nd–TiO_2 derived from XRD, UV Raman spectra, and N_2-adsorption.

Sample	Amount of Nd_2O_3 (wt%)	Crystallite size, D (nm)		Rutile content (%)		BET surface area (m^2/g)
		Anatase (1 0 1)	Rutile (1 1 0)	Bulk	Surface	
TiO_2-500 °C	0	20.2	–	0	0	52.3
TiO_2-800 °C	0	–	200[a]	100	100	5.8
Nd–TiO_2-500 °C	0.5	16.3	–	0	0	68.2
	3	12.2	–	0	0	89.7
Nd–TiO_2-800 °C	0.5	–	47.9	100	89.0	10.0
	3	29.9	34.7	72.0	52.0	15.2

[a] Particle size from TEM.

with TiO_2-500 °C, it is also observed that the characteristic bands of the anatase phase become broader and decrease in intensity for Nd–TiO_2-500 °C. It was suggested that the broadening of Raman peaks might be attributed to the three-dimensional confinement of phonons in the smaller size nanoparticles [29]. Combined with the results from the XRD patterns (Fig. 1a) and the UV Raman spectra (Fig. 1b), both the bulk and surface regions of TiO_2-500 °C and Nd–TiO_2-500 °C are in the anatase phase.

For both XRD and UV Raman spectroscopy, no peaks due to Nd_2O_3 crystalline phase are observed for Nd–TiO_2-500 °C. The radius of neodynium ions (0.995 Å) is larger than that of titanium ion (0.68 Å), possibly making it difficult for Nd^{3+} ion to be substituted into the lattice of TiO_2. Moreover, doping Nd^{3+} does not cause any shift in diffraction angles shown in Fig. 1a, suggesting that Nd^{3+} does not enter into the lattice structure of TiO_2 to replace the Ti^{4+} ion. The XRD result (figure is not shown) indicates that the crystal Nd_2O_3 can be obtained by calcining the $Nd(NO_3)_3{\cdot}6H_2O$ at 500 °C. These results indicate that Nd_2O_3 should be highly dispersed on the surface of a single TiO_2 grain or between the interfaces of TiO_2 agglomerates as Nd_2O_3 crystallites for Nd–TiO_2-500 °C [25]. The reduction in crystallite size of Nd–TiO_2-500 °C is proposed to be due to segregation of the neodymium cations at the grain boundary, which inhibits the grain growth by restricting direct contact of TiO_2 grains [30].

3.2. The bulk and surface crystalline phase of Nd–TiO_2-800 °C

XRD patterns and UV Raman spectra of TiO_2-800 °C and Nd–TiO_2-800 °C samples are shown in Fig. 2a and b. We conclude that the bulk region of TiO_2-800 °C and 0.5Nd–TiO_2-800 °C is in the rutile phase because only typical diffraction peaks due to rutile phase (27.6°, 36.1°, 41.2°, and 54.3°) [26] are observed. These results show that the phase transition from anatase to rutile in the bulk of TiO_2 is not effectively inhibited after 0.5 wt% Nd_2O_3 doping. The surface region of TiO_2-800 °C is in the rutile phase because only characteristic bands (143, 235, 445, and 612 cm^{-1}) due to rutile phase [28] are observed (Fig. 2b). The XRD (Fig. 2a) and UV Raman spectra (Fig. 2b) indicate that both the bulk and surface phase of TiO_2-800 °C are in the rutile phase. In other words, anatase totally transformed into the rutile phase when the calcination temperature is 800 °C.

However, for 0.5Nd–TiO_2-800 °C, its surface region is a main rutile phase with small amounts of anatase (11%) (Fig. 2b), while its bulk region is in the rutile phase (Fig. 2a). Compared with TiO_2-800 °C, the 0.5Nd–TiO_2-800 °C exhibits high anatase thermal stability in the surface region. It was found that the phase transformation of TiO_2 from anatase to rutile starts to occur at the interfaces of the contacting anatase grains (<60 nm) in the agglomerated TiO_2 particles [31]. The rutile phase nucleates in the inner region (bulk region) of the agglomerated TiO_2 particles and then develops to the outer region (surface region) of the agglomerated TiO_2 particles.

The formation of bulk rutile phase in 0.5Nd–TiO_2-800 °C cannot be effectively inhibited by 0.5 wt% Nd_2O_3 due to lower amount of dopant. However, the inhibition of the movement of Ti atoms or ionic oxygen mobility by the Nd_2O_3 additive may prohibit the development of the rutile phase. Thus, once the phase transformation starts, diffusion of rutile phase through the Nd_2O_3 doped TiO_2 may become difficult, i.e., the propagation of the rutile phase from the bulk into the surface region of Nd–TiO_2 is remarkably slowed by Nd_2O_3. This is the reason why the bulk region of 0.5Nd–TiO_2-800 °C is in the rutile phase, while its surface region is a mixture of anatase and rutile phases.

With increasing amounts of Nd_2O_3 up to 3 wt%, the typical peaks of anatase phase were also observed in the bulk region of 3Nd–TiO_2-800 °C, in addition to the diffraction peaks assigned to the rutile phase (Fig. 2a). It can be concluded that 3 wt% Nd_2O_3 can effectively prohibit the anatase crystallite aggregations, further prohibiting the phase transformation in the bulk region of 3Nd–TiO_2-800 °C. The phase transformation hindering might be attributed to the formation of strong Nd–O–Ti bonds, which inhibit the movement of Ti atoms required to initiate the phase transformation [32]. The weight fraction of the rutile phase in the TiO_2 sample, W_R, can be

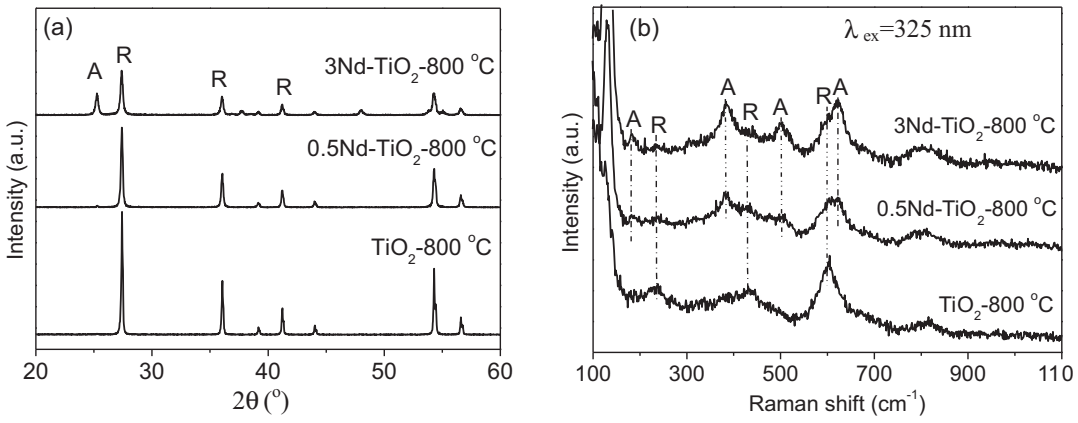

Fig. 2. The XRD patterns (a) and UV Raman spectra (b) of the TiO_2-800 °C and Nd–TiO_2-800 °C samples.

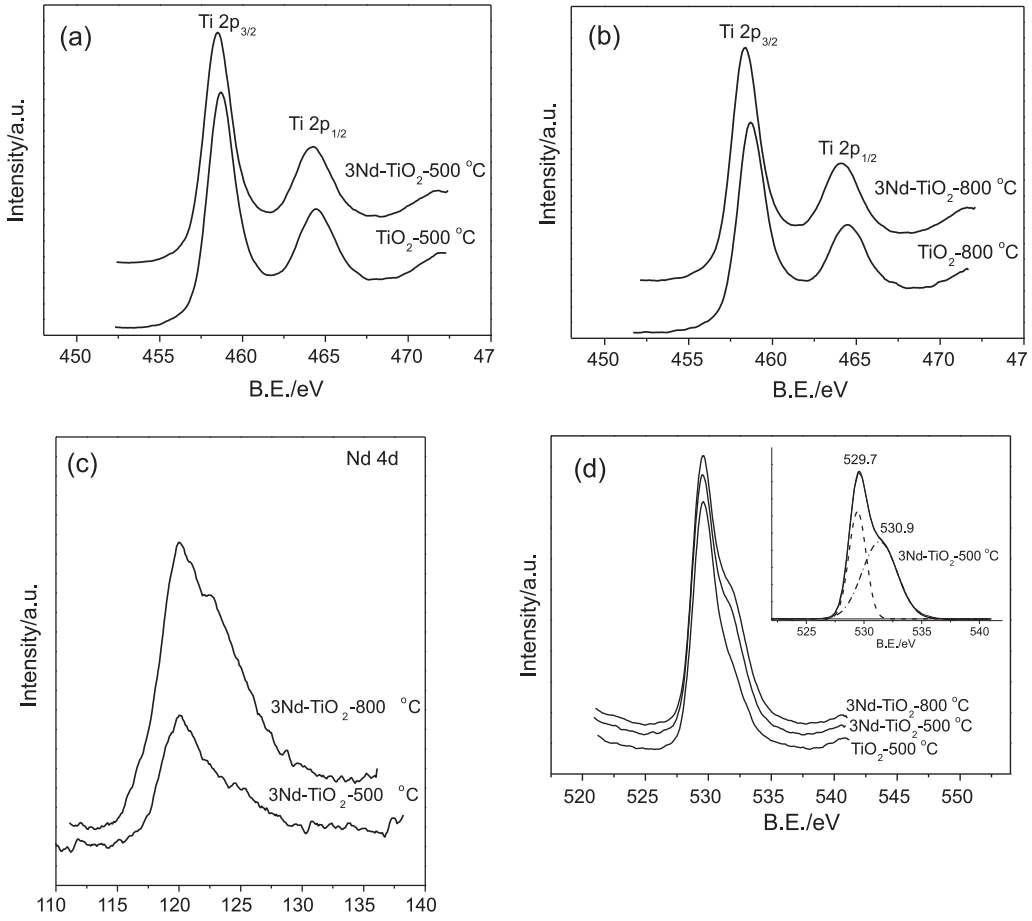

Fig. 3. XPS spectra of Ti 2p of TiO_2-500 °C and 3Nd–TiO_2-500 °C (a), Ti 2p of TiO_2-800 °C and 3Nd–TiO_2-800 °C (b), Nd 4d of 3Nd–TiO_2-500 °C and 3Nd–TiO_2-800 °C (c), O 1s of TiO_2-500 °C, 3Nd–TiO_2-500 °C and 3Nd–TiO_2-800 °C (d).

estimated from the XRD peak intensities using following formula [33]:

$$W_R = \frac{1}{[1 + 0.884(A_{ana}/A_{rut})]} \quad (1)$$

where A_{ana} and A_{rut} represents the X-ray integrated intensities of anatase (1 0 1) and rutile (1 1 0) diffraction peaks, respectively. The resulting rutile content in the bulk region of 3Nd–TiO_2-800 °C was calculated to be 72%.

Based on the UV Raman spectra (Fig. 2b), the content of the rutile phase in the surface region of Nd–TiO_2-800 °C is decreased from 89% to 52% when the amount of Nd_2O_3 is increased from 0.5 to 3 wt%. From the above results, it is easy to change the crystal phase and phase composition in bulk and surface region of the Nd–TiO_2 samples by changing the amount of Nd_2O_3. Further work is in progress to carefully control the surface and bulk crystalline phase of TiO_2 by Nd_2O_3 at high calcination temperatures.

3.3. XPS analysis

The XPS spectra of Ti 2p, O 1s, and Nd 4d of TiO_2 and 3Nd–TiO_2 samples calcined at different temperatures are shown in Fig. 3. In Fig. 3a and b, two peaks located at 458.4 eV and 464.1 eV were identified as Ti (2p3/2) and Ti (2p1/2), respectively. These results demonstrated that Ti elements existed mainly as 4+ valences in TiO_2 and 3Nd–TiO_2 calcined at 500 °C and 800 °C [34]. It is found that the presence of Nd_2O_3 exerts no significant influence on the XPS spectra in the Ti 2p level.

The XPS of Nd 4d (Fig. 3c) shows the Nd (4d 5/2) peak at about 121 eV which is quite consistent with Nd being typically present as Nd^{3+} (Nd_2O_3), suggesting that Nd element is present in the form of Nd_2O_3. According to XPS, the Nd/Ti atomic ratio was estimated to be 0.11 and 0.21 for 3Nd–TiO_2-500 °C and 3Nd–TiO_2-800 °C. The two Nd/Ti atomic ratios are significantly higher than the defined value (0.014). It confirms that most of the Nd_2O_3 crystallites distribute on the surface of TiO_2 grains or between the interfaces of TiO_2 agglomerates. Furthermore, it can be concluded that Nd^{3+} easily diffuses to the surface of the TiO_2 grains with increasing calcination temperature.

If we check the O in the XPS spectra for the TiO_2 system and the Nd–TiO_2 system (Fig. 3d), we see a shoulder and the O peak is completely asymmetric for the Nd–TiO_2 whereas for the TiO_2 system there is a single O1s peak at 529.7 eV. Upon deconvolution (see insert figure in Fig. 3d) of the O1s peak we find that there are two separate peaks at 529.7, 530.9 eV for the Nd–TiO_2 system. The peak at 529.7 eV is the characteristic peak of Ti–O bond [35]. The high-energy state (peak located at 530.9 eV) is assigned to O in Nd_2O_3 [35]. This proves that there are two different O-moieties in TiO_2 and Nd_2O_3. These results provide evidence that Nd^{3+} exist in individual phases. So along with the Ti 2p and Nd 4d, the O1s peak strongly suggests that the Nd^{3+} rather being substituted in the lattice sites of TiO_2 is present as an entirely separate phase.

3.4. TEM, SEM(EDX), and BET analysis

TEM was used to characterize the microstructure of the TiO_2-500 °C, TiO_2-800 °C, 3Nd–TiO_2-500 °C, and 3Nd–TiO_2-800 °C

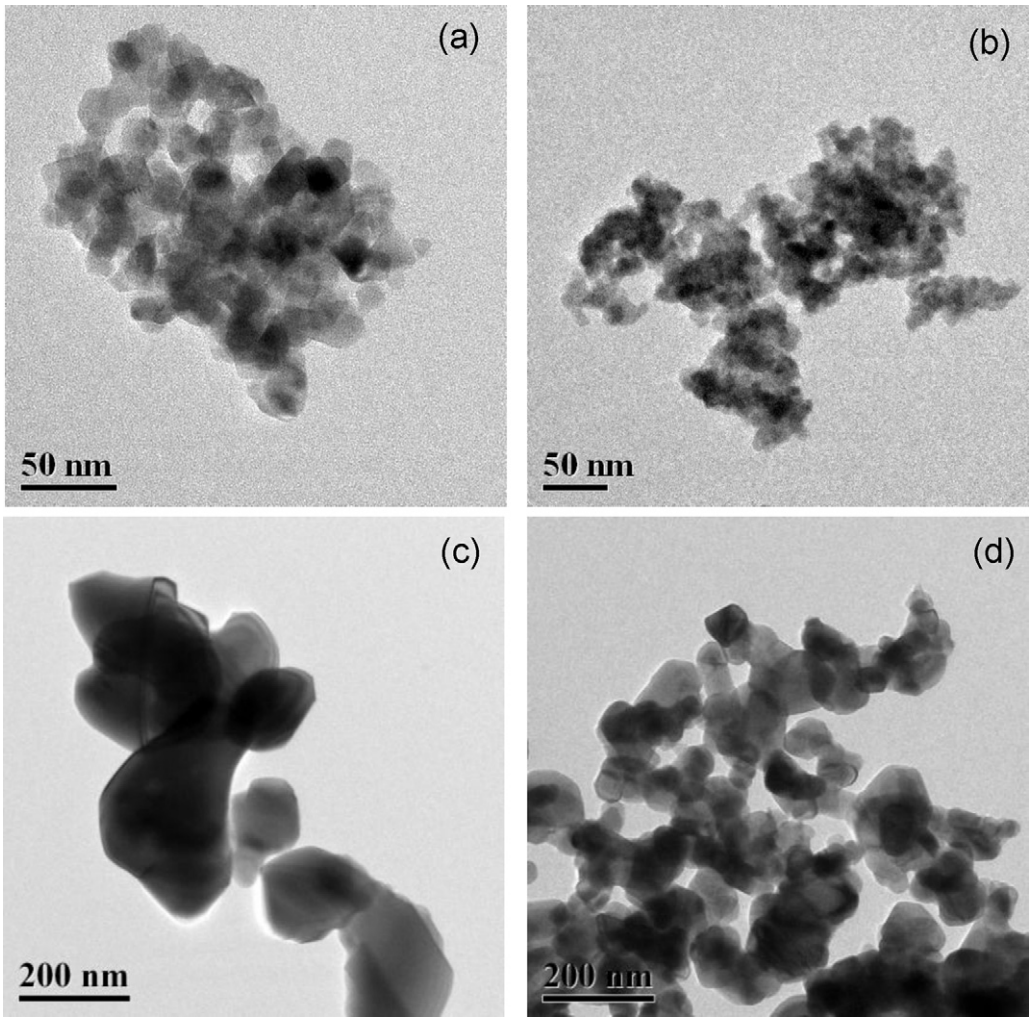

Fig. 4. TEM of TiO_2-500 °C (a), 3Nd–TiO_2-500 °C (b), TiO_2-800 °C (c), and 3Nd–TiO_2-800 °C (d).

(displayed in Fig. 4). The aggregation phenomena occurred in all the samples. TiO_2 and Nd–TiO_2 calcined at 500 °C and 800 °C display similar spherical form. 3Nd–TiO_2-500 °C (3Nd–TiO_2-800 °C) shows a smaller particle size than TiO_2-500 °C (TiO_2-800 °C), which is in accordance with the results from XRD and UV Raman spectroscopy (Figs. 1 and 2).

In comparison with TiO_2-500 °C, the particle size of TiO_2-800 °C increases obviously. From BET data, TiO_2-500 °C has a specific sur-

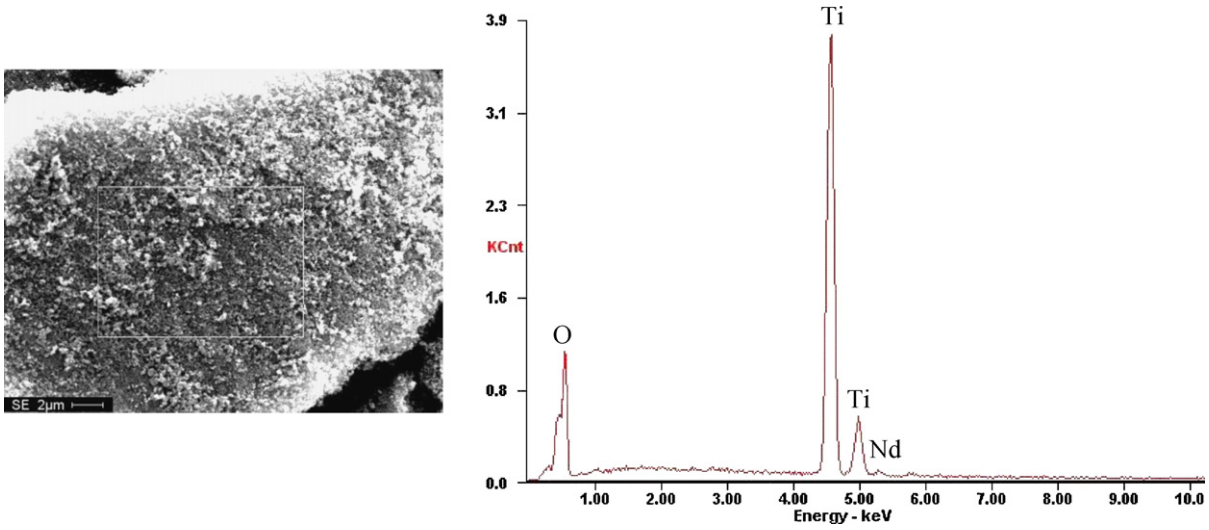

Fig. 5. Energy-dispersed X-ray (EDX) spectrum of 0.5Nd–TiO_2-500 °C sample.

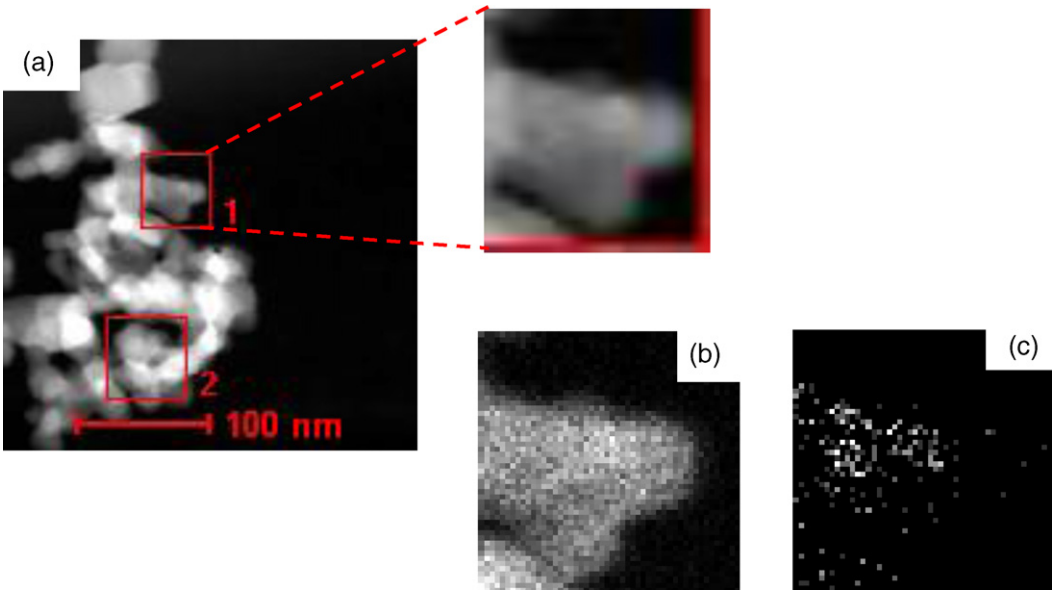

Fig. 6. STEM and EDX spectroscopy images of 0.5Nd–TiO_2-500 °C. (a) STEM image of 0.5Nd–TiO_2-500 °C, (b) EDX energy map of Ti corresponding to enlarge image of (a and c) EDX energy map of Nd corresponding to enlarge image of (a).

face area of 52.3 m^2/g and TiO_2-800 °C has a specific surface area of 5.8 m^2/g (Table 1). It is well known that the phase transformation of TiO_2 is accompanied by anatase crystallite aggregation, consequently increasing particle size of TiO_2 and decreasing surface area. It is obvious that Nd_2O_3 doping decreases particle size of TiO_2. As a result, the Nd–TiO_2 samples have significantly higher specific surface area than TiO_2 samples under the same calcination temperature (Table 1).

The SEM-EDX analysis is carried out to identify the elemental composition of 0.5Nd–TiO_2-500 °C, and the EDX spectrum has been shown in Fig. 5, which shows strong K diffraction peaks of elemental Ti at 4.51 and 4.95 keV, the K diffraction peak of elemental O at 0.52 keV [36]. Nd element was also detected by EDX analyses. According to the EDX results, the Nd/Ti atomic ratio was estimated to be 0.012 for 0.5Nd–TiO_2-500 °C. This value is higher than the defined value (2.3×10^{-4}). In addition, if we take the atomic ratio we get that of Ti is ~30 atom%. The O is ~70 atom%. For formation of TiO_2 the stoichiometric atom% of O required is ~60%. Therefore, the other 10 atom% of O might also be accounted for the formation of the Nd_2O_3.

For further investigation, an EDX mapping of the elements was carried out for 0.5Nd–TiO_2-500 °C. Fig. 6b and c are EDX energy maps of Ti element and Nd element respectively corresponding to the enlarge image of Fig. 6a. It is obvious that the distribution of Nd element is different from the distribution of Ti element. EDX elemental maps of samples for Ti and Nd show that Nd element does not homogeneously distribute in TiO_2 as the concentration of Nd is high near the surface of TiO_2 in the 0.5Nd–TiO_2-500 °C sample. Thereby in conjunction along with the XPS studies above, we can conclude from the EDX also that Nd^{3+} does not enter the TiO_2 lattice, but rather forms a separate oxide phase on the surface of TiO_2.

3.5. UV–visible diffuse reflectance spectra

To investigate the influence of Nd_2O_3 on the optical absorption properties of TiO_2, we examined the diffuse reflection adsorption spectra (DRS) of TiO_2 and Nd–TiO_2 samples calcined at 500 °C and 800 °C (Fig. 7a and b). The optical absorption of TiO_2 for wavelengths shorter than 390 nm is mainly attributed to the $O^{2-} \rightarrow Ti^{4+}$ charge-transfer, related to electron excitation from the valence band to the conduction band. [37]. In Fig. 7a, red shifts of the absorption edge toward the visible region are observed for doped samples. The red shifts can be attributed to the charge-transfer transition between earth ion f electrons and the TiO_2 conduction or valence

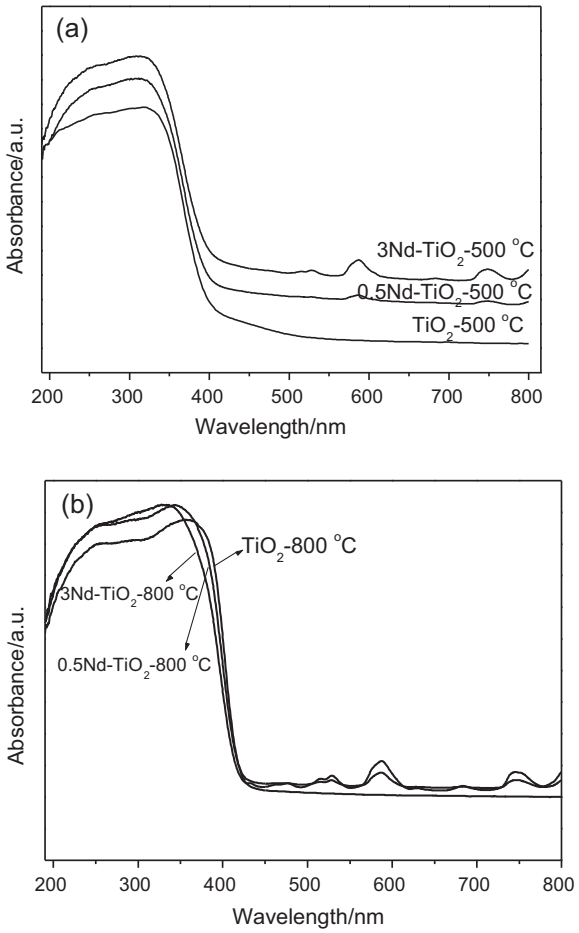

Fig. 7. UV–vis DRS spectra of TiO_2-500 °C and Nd–TiO_2-500 °C samples (a), TiO_2-800 °C and Nd–TiO_2-800 °C samples (b).

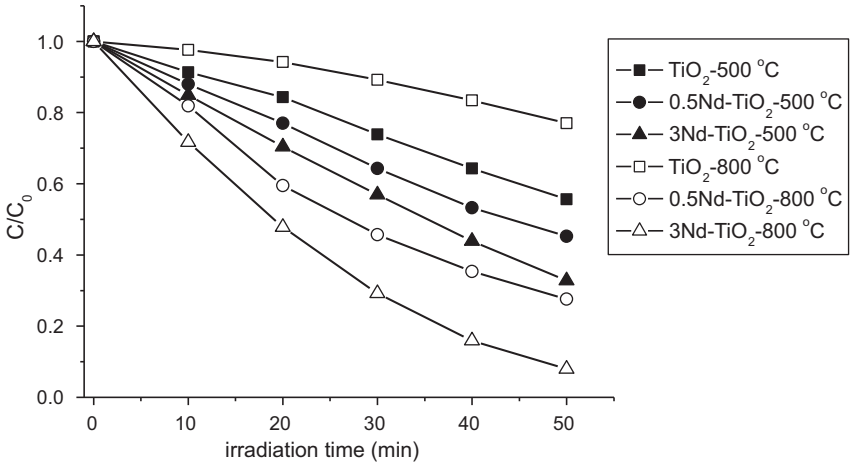

Fig. 8. The photocatalytic activity of degradation of Rhodamin B on the TiO_2 and Nd–TiO_2 photocatalysts calcined at different temperatures.

band [38,39]. With increased Nd^{3+} concentration, the absorption edge shifted to a longer wavelength.

The band-gap energies of TiO_2-500 °C and Nd–TiO_2-500 °C were estimated by DRS. By plotting $(\alpha E)^{1/2}$ vs E with α being the absorption coefficient, the band gap energies were calculated to be 3.22, 3.15, and 3.11 eV for TiO_2-500 °C, 0.5Nd–TiO_2-500 °C, and 3Nd–TiO_2-500 °C, respectively. This shows that Nd_2O_3 doping can narrow the band-gap of TiO_2, which may be beneficial for improving the photoabsorption and photocatalytic performance of TiO_2 [40]. Nd–TiO_2-500 °C catalyst had four typical absorption peaks in the visible region located at 527, 586, 762 and 802 nm [38], which corresponded to transitions of $4I_{9/2}$ to $2K_{13/2}$ and $4G_{7/2}$, $2G_{7/2}$ and $4G_{5/2}$, $4S_{3/2}$ and $4F_{7/2}$, $4F_{5/2}$ and $2H_{9/2}$, respectively [41]. Moreover, the intensities of these absorption bands were found to increase with increasing in rare earth content.

For Nd–TiO_2-800 °C samples (Fig. 6b), the maximum absorption shows a blue shift with increasing the Nd_2O_3 contents. The maximum absorption is at 359 nm for TiO_2-800 °C, 343 nm for 0.5 Nd–TiO_2-800 °C, and 332 nm for 3Nd–TiO_2-800 °C. As discussed in Section 3.2, the contents of the anatase phase in Nd–TiO_2-800 °C increase with increased doping of Nd_2O_3. Thus, the gradual blue shift in the maximum absorption of Nd–TiO_2-800 °C is in good agreement with increase of anatase contents with increasing Nd_2O_3 content.

3.6. Evaluation of photocatalytic activity of the samples

RhB was used as the representative organic substances to evaluate the photoactivity of TiO_2-500 °C, TiO_2-800 °C, Nd–TiO_2-500 °C, and Nd–TiO_2-800 °C samples (Fig. 8). The degradation of RhB could be described by first-order kinetic of $-\ln(C_t/C_0)$ vs reaction time (t):

$$-\ln\left(\frac{C_t}{C_0}\right) = k_{ap}t \quad (2)$$

where k_{ap} is the apparent reaction rate constant, C_0 and C_t are the initial concentration and the concentration of RhB at reaction time t, respectively. After 50 min of irradiation, 55% and 67% of RhB are degraded by the 0.5Nd–TiO_2-500 °C and 3Nd–TiO_2-500 °C catalysts as compared to 44% by the TiO_2-500 °C photocatalyst. This suggests that Nd^{3+} doping enhances the photocatalytic activity of TiO_2.

The BET results (Table 1) show that the specific surface areas increased from 52.3 m^2/g for TiO_2-500 °C to 68.3 m^2/g for 0.5Nd–TiO_2-500 °C, and then to 89.7 m^2/g for 3Nd–TiO_2-500 °C. Usually, a large specific surface area may be an important factor, influencing the rate of photocatalytic degradation reaction, as a large amount of adsorbed organic molecules promote the photocatalytic reaction. Therefore, the larger specific surface area of Nd–TiO_2-500 °C photocatalysts provides more absorbing sites for reactant molecules (RhB) [42]. Moreover, the decrease in the particle size of Nd–TiO_2-500 °C enhances the photoinduced charge transfer from the bulk of particles to the surface-absorbed reactants [43]. Xu et al. [43] suggested the 4f level of lanthanide plays an important role in interfacial charge transfer and elimination of electron–hole recombination for lanthanide-doped sample. Lanthanide ions could act as an effective electron scavenger to trap the CB electrons of TiO_2.

As discussed above, neodymium doping has little influence on the surface and bulk crystalline phase of Nd–TiO_2-500 °C samples while has an obvious influence on the surface areas and optical absorption properties of Nd–TiO_2-500 °C samples. Although the Nd–TiO_2-500 °C samples have the same surface phase as the TiO_2-500 °C sample, they exhibit a different overall rate of photocatalytic degradation of RhB (Table 2). This trend in photocatalytic activity of degradation of RhB is different from that of the rate of H_2 production (from the photocatalytic reaction of water and methanol), which the overall photocatalytic activity does not evidently change for TiO_2 samples with the surface anatase phase. For Nd–TiO_2 with the same surface anatase phase, surface area and the optical absorption properties of Nd–TiO_2 are the two main factors influence its photocatalytic activity of degradation of RhB.

Compared with TiO_2-500 °C, the decrease in particle size, increase in surface area, extension of optical range, and increase in the separation efficiency of electron–hole pairs of Nd–TiO_2-500 °C are the reasons for the higher photocatalytic activity of Nd–TiO_2-500 °C. In addition, Shah et al. [44] proposed that the high oxygen affinities of interstitially located Nd^{3+} ions effectively create a localized positive charge around Ti and/or form an oxygen vacancy. The potential energy of ion dopants was disturbed and electrons were efficiently trapped. Consequently, the photocatalytic activity was remarkably improved.

Table 2
The first-order kinetic constants (k_{ap}, min^{-1}) and relative coefficient (R^2) for degradation of RhB under UV light irradiation.

	TiO_2-500 °C	0.5Nd–TiO_2-500 °C	3Nd–TiO_2-500 °C	TiO_2-800 °C	0.5Nd–TiO_2-800 °C	3Nd–TiO_2-800 °C
Apparent rate constant, k_{ap} (min^{-1})	0.01175	0.01615	0.02219	0.00524	0.02635	0.05044
Relative coefficient (R^2)	0.9933	0.9973	0.9941	0.9802	0.9989	0.9910

TiO_2-800 °C showed poor photocatalytic performance with a k_{ap} of 0.00524 min^{-1} (Table 2), this is due to the rutile phase in the bulk and surface region and its small specific surface areas (5.8 m^2/g). Rutile TiO_2 shows a much higher combination rate of photo-generated electrons and holes compared with the anatase phase [45]. 0.5Nd–TiO_2-800 °C shows much higher activity with a k_{ap} of 0.02635 min^{-1} than TiO_2-800 °C, implying that modification with Nd_2O_3 can improve the photocatalytic degradation rate of RhB. As discussed above, the enhanced activity of 0.5Nd–TiO_2-800 °C is attributed to its high surface area and its high separation efficiency of electron–hole pairs, resulting from the addition of Nd_2O_3.

It should be noted that the 0.5 Nd–TiO_2-800 °C has slightly higher band gap energy than TiO_2-800 °C. Moreover, the specific surface areas of 0.5Nd–TiO_2-800 °C (10.0 m^2/g) are comparable to that of TiO_2-800 °C (5.8 m^2/g). However, the activity of 0.5Nd–TiO_2-800 °C is greatly improved. UV Raman spectra results (Fig. 2b) indicated that the surface region of 0.5Nd–TiO_2-800 °C is in the mixed phase compositions with 11% anatase and 89% rutile phase, while the surface region of TiO_2-800 °C is in the pure rutile phase. It is clear that the photocatalytic activity of 0.5Nd–TiO_2-800 °C drastically increased with a small amount of anatase phase in the surface region compared to pure surface rutile phase (TiO_2-800 °C).

It is interesting to note that despite the larger surface area of 0.5Nd–TiO_2-500 °C, 0.5Nd–TiO_2-800 °C has the higher activity. Mixed surface phases of anatase and rutile (89% rutile and 11% anatase) are observed for 0.5Nd–TiO_2-800 °C (Fig. 1b), while pure surface anatase phase is observed for 0.5Nd–TiO_2-500 °C (Fig. 2b). These results imply that 0.5Nd–TiO_2-800 °C with a mixture of surface anatase and rutile has a higher rate of photocatalytic degradation of RhB than pure surface anatase or pure surface rutile TiO_2. These results strongly suggest the existence of a synergistic effect between surface anatase and rutile phase in the Nd^{3+} doped TiO_2, which is similar to that of undoped TiO_2 [22]. This synergistic effect (formation of the surface anatase/rutile phase junction) favors photoinduced charge separation [16–18], and further improves the rate of photocatalytic degradation of RhB.

For 3Nd–TiO_2-800 °C, the surface rutile and anatase content is about 52 and 48%, respectively. Compared with 0.5Nd–TiO_2-500 °C, containing 89% rutile and 11% anatase in the surface region, the amount of the anatase/rutile phase junction on the TiO_2 surface may increase for the 3Nd–TiO_2-800 °C. Thus, the higher photocatalytic degradation of RhB for 3Nd–TiO_2-800 °C is observed. In short, the introduction of Nd_2O_3 into TiO_2 inhibits the growth of particle size, phase transition, extends the optical range, creates a localized positive charge around Ti and/or forms an oxygen vacancy, and increases the amount of the phase junctions between anatase and rutile in the surface region. This may give rise to a high photoactivity of degradation of Rhodamine B for 3Nd–TiO_2-800 °C.

4. Conclusions

TiO_2 modified with Nd_2O_3 (Nd–TiO_2) nanoparticles were synthesized using a co-precipitation method. A systematic characterization involving bulk and surface crystal structure, particle size, specific surface area, chemical state of neodynum dopant, and optical properties of Nd–TiO_2, together with their relationships with the photocatalytic degradation of Rhodamine B (RhB) were conducted. It was found that Nd^{3+} does not enter TiO_2 lattice, but exists in individual phases in the form of Nd_2O_3 on the surface of TiO_2 grains or the interface of TiO_2 agglomerated particles. Moreover, Nd^{3+} easily diffused to the surface of TiO_2 grains or the interface of TiO_2 agglomerated particles with increasing calcination temperature. The surface modification with Nd_2O_3 can enhance the thermal stability of the anatase phase in the surface region of Nd–TiO_2.

For the Nd–TiO_2 samples with the same surface anatase phase, the activity enhancement of Nd–TiO_2 is mainly attributed to the high photoinduced charge separation rate, large surface area, and to the extension of optical response range. For the Nd–TiO_2 samples with the mixed phases of anatase and rutile in the surface region, a synergistic effect was found between surface anatase and rutile phase, which is similar to that of undoped TiO_2. This paper provides a strategy for designing high-performance TiO_2-based photocatalysts for photodegradation of organic pollution by tuning the surface phase composition and keeping a large surface area.

Acknowledgments

This work was supported by the National Nature Science Foundation of China (No. 20903054). We thank Associate Professor Xuming Wei from State Key Laboratory of Catalysis, Dalian Institute of Chemical Physics, Chinese Academy of Sciences for assistance with STEM measurements and analysis. We also thank Alex Peroff and Kaustava Bhattacharyya from Department of Chemistry, Northwestern University for improving the English in the manuscript.

References

[1] J. Zheng, Z. Liu, X. Liu, X. Yan, D. Li, W. Chu, J. Alloys Compd. 509 (2011) 3771–3776.
[2] S. Mahshida, M. Askaria, M. Sasani Ghamsarib, N. Afsharc, S. Lahutic, J. Alloys Compd. 478 (2009) 586–589;
V. Puddu, H. Choi, D.D. Dionysiou, G.L. Puma, Appl. Catal. B: Environ. 94 (2010) 211–218.
[3] L. Baia, L. Diamandescu, L. Barbu-Tudoran, A. Peter, G. Melinte, V. Danciu, M. Baia, J. Alloys Compd. 509 (2011) 2672–2678.
[4] Mst.S. Nahara, J. Zhang, K. Hasegawa, S. Kagaya, S. Kuroda, Mater. Sci. Semicond. Process 12 (2009) 168–174.
[5] K.V. Baiju, P. Periyat, P. Shajesh, W. Wunderlich, K.A. Manjumol, V.S. Smitha, K.B. Jaimy, K.G.K. Warrier, J. Alloys Compd. 505 (2010) 194–200.
[6] (a) T. Ohno, K. Sarukawa, M. Matsumura, J. Phys. Chem. B 105 (2001) 2417–2420;
(b) Y. Sakatani, D. Grosso, L. Nicole, C. Boissiere, G. Soler-Illia, C. Sanchez, J. Mater. Chem. 16 (2006) 77–82.
[7] Y. Li, N.H. Lee, E.G. Lee, J.S. Song, S.J. Kim, Chem. Phys. Lett. 389 (2004) 124–128.
[8] S.S. Watson, D. Beydoun, J.A. Scott, R. Amal, Chem. Eng. J. 95 (2003) 213–220.
[9] M.H. Habibi, H. Vosooghian, J. Photochem. Photobiol. A 174 (2005) 45–52.
[10] A. Sclafani, L. Palmisano, M. Schiavello, J. Phys. Chem. 94 (1990) 829–832.
[11] Y. Liao, W. Que, Z. Tang, W. Wang, W. Zhao, J. Alloys Compd. 509 (2011) 1054–1059.
[12] Y.K. Kho, A. Iwase, W.Y. Teoh, A. L.Mädler, R.A. Kudo, J. Phys. Chem. C 114 (2010) 2821–2829.
[13] G. Li, S. Ciston, Z.V. Saponjic, L. Chen, N.M. Dimitrijevic, T. Rajh, K.A. Gray, J. Catal. 253 (2008) 105–110.
[14] A. Zachariah, K.V. Baiju, K.S. Deepa, J. James, K.G.K. Warrier, J. Phys. Chem. C 112 (2008) 11345–11356.
[15] A.M. Luís, M.C. Neves, M.H. Mendonça, O.C. Monteiro, Mater. Chem. Phys. 125 (2011) 20–25.
[16] T. Kawahara, Y. Konishi, H. Tada, N. Tohge, J. Nishii, S. Ito, Angew. Chem. Int. Ed. 41 (2002) 2811–2813.
[17] K. Komaguchi, H. Nakano, A. Araki, Y. Harima, Chem. Phys. Lett. 428 (2006) 338–342.
[18] A. Di Paola, M. Bellardita, R. Ceccato, L. Palmisano, F. Parrino, J. Phys. Chem. C 113 (2009) 15166–15174.
[19] N.L. Wu, M.S. Lee, Z.J. Pon, J.Z. Hsu, J. Photochem. Photobiol. A: Chem. 163 (2004) 277–280.
[20] J. Zhang, M.J. Li, Z.C. Feng, J. Chen, C. Li, J. Phys. Chem. B 110 (2006) 927–936;
W.G. Su, J. Zhang, Z.C. Feng, T. Chen, P.L. Ying, C. Li, J. Phys. Chem. C 112 (2008) 7710–7716.
[21] J. Zhang, Q. Xu, Z.C. Feng, M.J. Li, C. Li, Angew. Chem. Int. Ed. 47 (2008) 1766–1769.
[22] G.Q. Wang, W. Lan, G.J. Han, Y. Wang, Q. Su, X.Q. Liu, J. Alloys Compd. 509 (2011) 4150–4153.
[23] S. Chang, W. Liu, Appl. Catal. B: Environ. 101 (2011) 333–342.
[24] (a) J.J. Xu, Y.H. Ao, D.G. Fu, C.W. Yuan, Colloids Surf. A: Physicochem. Eng. Aspects 334 (2009) 107–111;
(b) A.W. Xu, Y. Gao, H.Q. Liu, J. Catal. 207 (2002) 151–157.
[25] J.J. Zou, B. Zhu, L. Wang, X. Zhang, Z. Mi, J. Mol. Catal. A: Chem. 286 (2008) 63–69.
[26] T. Sreethawong, Y. Suzuki, S. Yoshikawa, J. Solid State Chem. 178 (2005) 329–338.
[27] F.B. Li, X.Z. Li, K.H. Ng, Ind. Eng. Chem. Res. 45 (2006) 1–7.
[28] T. Ohsaka, F. Izumi, Y. Fujiki, J. Raman Spectrosc. 7 (1978) 321–324.
[29] V. Swamy, A. Kuznetsov, L.S. Dubrovinsky, R.A. Caruso, D.G. Shchukin, B.C. Muddle, Phys. Rev. B 71 (2005), 184302-1-184302-11.

[30] X. Ding, X. Liu, J. Mater. Res. 13 (1998) 2556–2559.
[31] J. Zhang, Q. Xu, M.J. Li, Z.C. Feng, C. Li, J. Phys. Chem. C 113 (2009) 1698–1704.
[32] A.M. Ruiz, G. Dezanneau, J. Arbiol, A. Cornet, J.R. Morante, Chem. Mater. 16 (2004) 862–871.
[33] A.A. Gribb, J.F. Banfield, Am. Miner. 82 (1997) 717–728.
[34] L.Q. Jing, Z.L. Xu, J. Shang, X.J. Sun, W.M. Cai, H.G. Fu, Sol. Energy Mater. Sol. Cells 79 (2003) 133–151.
[35] (a) Y.F. Ma, J.L. Zhang, B.Z. Tian, F. Chen, L.Z. Wang, J. Hazard. Mater. 182 (2010) 386–393;
(b) T.M. Pan, T.Y. Yu, Semicond. Sci. Technol. 24 (2009) 095022.
[36] Z.H. Zhang, Y. Yuan, L.H. Liang, Y.X. Cheng, G.Y. Shi, L.T. Jin, J. Hazard. Mater. 158 (2008) 517–522.
[37] L.Q. Jing, B.F. Xin, F.L. Yuan, L.P. Xue, B.Q. Wang, H.G. Fu, J. Phys. Chem. B 110 (2006) 17860–17865.
[38] V. Štengl, S. Bakardjieva, N. Murafa, Mater. Chem. Phys. 114 (2009) 217–226.
[39] E. Borgarello, J. Kiwi, M. Gratzel, E. Pelizzetti, M. Viscald, J. Am. Chem. Soc. 104 (1982) 2996–3002.
[40] L.Q. Jing, J. Wang, Y.C. Qu, Y.B. Luan, Appl. Surf. Sci. 256 (2009) 657–663.
[41] C. Koepke, K. Wisniewski, L. Sikorski, D. Piatkowski, K. Kowalska, M. Naftaly, Opt. Mater. 28 (2006) 129–136.
[42] Q. Xiao, Z.C. Si, Z.M. Yu, G.Z. Qiu, Mater. Sci. Eng. B 137 (2007) 189–194.
[43] J.J. Xu, Y.H. Ao, D.G. Fu, C.W. Yuan, J. Hazard. Mater. 164 (2009) 762–768.
[44] S.I. Shah, W. Li, C.P. Huang, O. Jung, C. Ni, PNAS 99 (2002) 6482–C6486.
[45] K. Lv, J. Yu, K. Deng, X. Li, M. Li, J. Phys. Chem. Solids 71 (2010) 519–522.